crystals

MDPI

Article

Perturbed Angular Correlation Technique at ISOLDE/CERN Applied for Studies of Hydrogenated Titanium Dioxide (TiO_2): Observation of Cd-H Pairs

Dmitry V. Zyabkin [1,*], Juliana Schell [2,3], João G. M. Correia [2,4], Ulrich Vetter [1] and Peter Schaaf [1]

[1] Materials for Electrical Engineering and Electronics Department, Institute of Materials Science and Engineering, Institute of Micro and Nanotechnology MacroNano®, TU Ilmenau, Gustav-Kirchhoff-Strasse 5, 98693 Ilmenau, Germany; vetter@nagl-vetter.de (U.V.); peter.schaaf@tu-ilmenau.de (P.S.)
[2] European Organization for Nuclear Research (CERN), CH-1211 Geneva, Switzerland; juliana.schell@cern.ch (J.S.); guilherme.correia@cern.ch (J.G.M.C.)
[3] Center for Nanointegration Duisburg-Essen (CENIDE), Institute for Materials Science, University of Duisburg-Essen, 45141 Essen, Germany
[4] Centro de Ciências e Tecnologias Nucleares, Departamento de Engenharia e Ciências Nucleares, Instituto Superior Técnico, Universidade de Lisboa, Bobadela, 2695-066 Boticas, Portugal
* Correspondence: dmitry.zyabkin@tu-ilmenau.de

Abstract: Profound understanding of the local electronic and defect structure in semiconductors always plays a vital role in the further developing of applications of such materials. In the present work an investigation of the electronic structure in hydrogenated TiO_2 (rutile) thin films is conducted by virtue of Time-Differential γ-γ Perturbed Angular Correlation spectroscopy (TDPAC or PAC) with ^{111m}Cd/Cd isotope, produced and implanted at ISOLDE/CERN. The measurements were performed at 581 K as a function of the temperature of the samples during hydrogenation. Despite the fact, that rutile single crystals usually show the presence of two local environments, when are studies with Cd/In isotopes, the current pristine thin films sample had a single electric field gradient. Upon various degrees of hydrogenation, Cd probe atoms showed underwent alterations, resulting in up to 3 different local surroundings, generally with high electric field gradients. Broad EFG distributions are likely due to randomly distributed point defects in the neighbourhood of Cd acceptors. Observed results suggest that hydrogenations performed at RT and 423 K are not able to promote unique defect configurations, while in the range of 473-573 K the formation of such configurations is observed. Therefore, one may assume that the formation of Cd-defect complexes (Cd-H pairs) is temperature enhanced. At higher levels of hydrogenation (663 K), the samples become partly amorphous that further hinders any atomistic studies with strong damped PAC spectra. Cd-H complexes seem to be stable up to annealing up to 581 K annealing. The obtained results give a deep insight into complex hydrogen defects, their interactions and bond formations with Cd acceptor.

Keywords: TiO_2; rutile; hydrogen; perturbed angular correlations; ion implantation; nuclear solid-state physics

Citation: Zyabkin, D.V.; Schell, J.; Correia, J.G.M.; Vetter, U.; Schaaf, P. Perturbed Angular Correlation Technique at ISOLDE/CERN Applied for Studies of Hydrogenated Titanium Dioxide (TiO_2): Observation of Cd-H Pairs. *Crystals* **2022**, *12*, 756. https://doi.org/10.3390/cryst12060756

Academic Editors: José L. Arias

Received: 22 March 2022
Accepted: 18 May 2022
Published: 24 May 2022

1. Introduction

Hydrogen is a well known impurity in semiconductors with prominent impact on electrical, structural and optical properties. Intentional hydrogen incorporation (generally by plasma or implantation) allows tuning the bandgap and consequently improves solar light absorption caused by both reduction of ions and hydrogen doping [1]. Behaviour of hydrogen in semiconductors is far from being straightforward. Despite a multitude of possible states (H^+, H^-, H^0 and H_2) hydrogen can take, there is a mere handful of information available, even for most used compounds. Depending on a semiconductor, hydrogen behaves differently. In wide-band-metal-oxides, hydrogen tends to bound to oxygen and can mainly act as an amphoteric impurity or as a donor [2]. The latter is the

case for TiO_2. In stable rutile, oxygen vacancies are also considered contributing to the system. However, when there is an excess of electrons they tend to be localised at the Ti site, giving rise to a polaron formation. Moreover, a polaron remains favourable even when additional electrons are induced via a dopant [3,4]. In the 70s, an improvement of *n*-type conductivity was spotted after hydrogenation in TiO_2. Interstitial hydrogen was suggested to form a single dative bond to an oxygen atom, where hydrogen was located in the open *c* channel of the crystal [5].

More recent studies with IR absorption spectroscopy have shown that the hydrogen nature in metal oxides is far more complicated. It has been shown that hydrogen could feature several forms stable against low temperature annealing, and furthermore, if it is stabilised by a defect nearby can remain in the lattice up to 1150 K [6–9]. Stability of these complexes against other impacts (*e.g.* ion implantation, stress) raises questions. Under IR and electron irradiation, diffusivity of hydrogen has significantly improved and is anisotropic, with the activation barrier remarkable lower in the *c*-direction [10,11].

One of the subtle methods to probe structure, electronic properties and stability of impurity complexes in solids at the atomic scale is perturbed angular correlation spectroscopy. PAC is sensitive to the local electric field gradients (EFG) present in the lattice near the probe atom. Not only the method provides the information on structure and stability, it also allows spotting dynamical processes (correlation times in the order of μs or even ns), which is of big help for fast diffusion phenomena and fluctuation of charge states. An electric field gradient is caused by a charge distribution, which deviates from an ideal spherically symmetric arrangement around the implanted probe. The EFG is usually described by the quadrupole coupling constant $\nu_Q = eQ\,V_{zz}/h$ (here Q is nuclear quadrupole moment and V_{zz} is the largest component of the EFG tensor) and asymmetry parameter, η. The latter can only take values between 0 and 1, and measures how far from axial symmetry a charge distribution deviates: $\eta = (V_{xx} - V_{yy})/V_{zz}$. In the current study, we are going to use $\omega_0 = \nu_Q * (3\pi/10)$ as the spin of the Cd 245 keV probe state is $I = 5/2^+$. When $\eta \simeq 0$ due to the high symmetry of the lattice and/or complex defects $\omega_0 = \omega_1$ is the smallest of the three observable frequencies characterising each EFGs, as $\omega_3 = \omega_1 + \omega_2$ for $I = 5/2$. More details about the method can be found elsewhere [12]. The only significant bottleneck of the method is few suitable isotopes. However, ISOLDE/CERN facility provides the user with a great variety of suitable short-lived isotopes [13].

The method has been previously applied for studying acceptor complexes, passivation, influence of pressure and annealing on hydrogen bonds dissociation and impact of hydrogen on the electric field gradient in semiconductors (Si, GaP, InP, and InAs) [14]. In those studies hydrogen was introduced in several ways, including hydrogen plasma or low energy implantation. In the case of Si, for instance, hydrogen formed pairs with the majority of impurity probes (up to 80%) and its incorporation in the lattice did not influence the axial asymmetry parameter, η, of the EFG, and only alterations of the main observable ω_0 frequencies evidenced the changes [15]. Studies performed with another hyperfine interaction method - ^{57}Fe emission Mössbauer spectroscopy on hydrogen plasma treated anatase samples have shown that hydrogen complexes are likely to be featured in at least two main forms: interstitial (or weakly bounded with longer bonds) $H_I^\bullet$ and hydrogen with a covalent bond to an oxygen atom $H_C^\bullet$. These complexes have different activation energy, and thus their thermal motion was triggered in two consequent steps: (1) $H_I^\bullet$ moves through equivalent positions (2) $H_C^\bullet$, once activation energy is sufficient to break its bond [16]. In the case of highly doped and V_o-abundant samples, both steps could overlap. Therefore, it would be of big interest to go through these steps with PAC spectroscopy, as it provides several advantages over Mössbauer spectroscopy, especially at elevated temperatures. However, within the present study we performed several PAC experiments with ^{111m}Cd probes on TiO_2 anatase samples and obtained no perturbations, as it also happened in the case of ^{111}Ag/Cd isotope [17]. The reason behind the flat response of the perturbation function in anatase could be attributed to the formation of different charge states of the daughter probe, thus leading to a tiny V_{zz}, and consequently causing

no perturbation of the time spectrum. Correspondingly, as pristine rutile behaves similarly, as anatase does [16,18], here we aim to spot ongoing changes in the electronic structure of hydrogenated rutile and to follow the behaviour of various environments on the verge between the first and second dissociation stages (in the vicinity of 570-580 K) [9,16].

2. Materials and Methods

TiO_2 thin films were prepared by radio frequency sputtering (LA 440S by VON ARDENNE) onto 1 × 1 cm Si substrates, utilising a ceramic TiO_2 target (99.9% FHR Anlagenbau, Germany). During the process, the sputtering power was kept at 210 W and the Ar flux was fixed at 80 sccm. The thickness of thin films was controlled with an ellipsometer (Sentech SE 801) and was in order of 500 nm. Prior to hydrogenation, the samples were annealed at 1073 K for 5 h with slow cooling, to ensure their full crystallisation into rutile. Thereafter, the samples were treated in a chamber for plasma-enhanced hydrogenation, where an inductively coupled plasma instrument (Plasma Lab 100 ICP-CVD, Oxford Instruments) was used. The H_2 plasma treatment was performed for 30 min in a broad temperature range of the substrate specifically at: room temperature (RT), 423, 473, 573 and 663 K. The ICP power was held at 3000 W, the chamber pressure at 3.5 Pa, and the H_2 flow rate at 50 sccm.

PAC experiments were carried out on a basis of 6-detector TDPAC spectrometer equipped with $LaBr_3$ detectors placed around a tubular furnace at 90° geometry with time resolution (800 ps) [19]. Isotopes of ^{111m}Cd/Cd were implanted at room temperature into samples with energy of 30 keV and fluence in the order of 1.1×10^{11} at/cm^2 provided by the ISOLDE radioactive beam facility at CERN [20]. Usually, each sample is measured once, with a repetition if statistical quality is not sufficient. Since, the hydrogenation was done prior to the implantation, the radiation-damage-recovery-annealings were performed during the measurements up to a certain extent. This decision was based on an earlier study of implantation damage in rutile, where approximately a significant amount of the total damage was recovered near 500 K [21], with the majority of damage affected in the near surface regions.

The chosen ^{111m}Cd isotope decays to ^{111}Cd via a cascade of two consecutive gamma rays of 151–245 keV, without inducing electronic excitation of the probe atom. The intermediate state has a lifetime $t_{1/2}$ = 85 ns, while the parent state decays with $t_{1/2}$ = 48.5 min. SRIM calculations [22]) showed that the depth of implantation should not exceed 30 nm (average 15 nm). Quadrupole moment used for determination of the EFG (V_{zz}) is 0.664(7)b [23].

X-ray diffraction patterns were recorded with a SIEMENS/BRUKER D 5000 X-ray diffraction using Cu-Kα radiation at 40 kV and 40 mA, with a pristine sample being scanned from 20° to 80° with a step size of 0.02° in Grazing incidence (GIXRD).

3. Results and Discussions

Figure 1 shows the observable R(t) spectra and their Fourier transforms, as measured at 581 K after implantation of ^{111m}Cd, for pristine and several TiO_2 samples hydrogenated at different temperatures. Table 1 summarises the fitting parameters of the main fractions of ^{111}Cd probe nuclei interacting with different EFG distributions. Description of the results is divided into sections to facilitate the discussion flow.

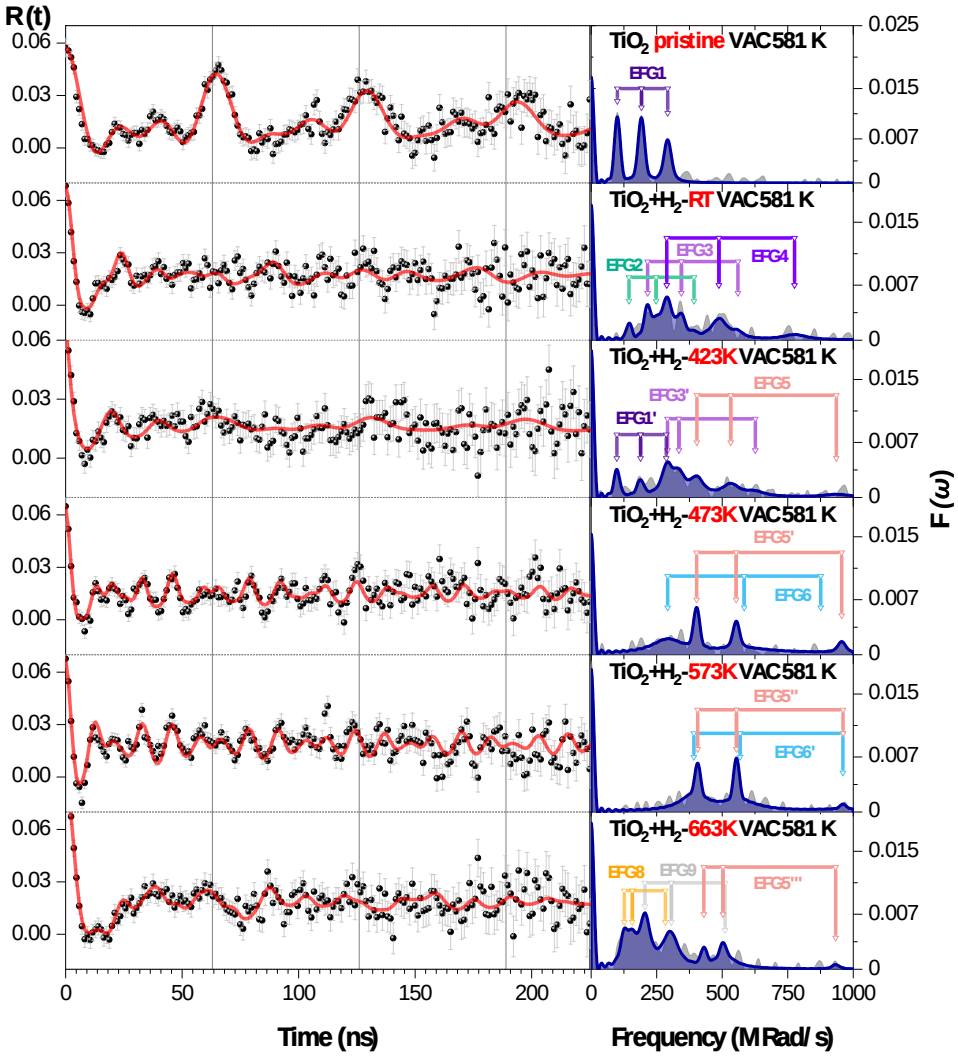

Figure 1. PAC spectra as a function of hydrogenation temperature with the corresponding Fourier transforms. Solid lines are the least-squares fit of the appropriate theoretical function to the experimental data.

3.1. Pristine Rutile

Annealing at 581 K seems to be sufficient to recover most of the implantation damage of the pristine sample, where solely one fraction of a single triplet of frequencies is seen to be present in the corresponding R(t) Fourier spectrum. The corresponding R(t) function has a well-defined pattern, what is the characteristic of a single EFG/environment for the Cd atoms in TiO_2, being only slightly damped as a function of time. The electric field gradient (EFG 1) resembles the values previously obtained on rutile [24,25]. Absence of significant remaining implantation damage is evidenced by several factors. Firstly, one points to the small damping of the R(t) function that reveals a low density of defects, with an essentially defect free local environment. Secondly, the main frequency measured at this temperature ω_{01} = 96.52(3) Mrad·s^{-1} matches closely with previously reported values on rutile with Cd isotope [24,26] ω_0 = 98.5(2) Mrad·s^{-1}.

The non-zero axially asymmetry parameter resembles results already measured at room temperature, although being slightly higher (η = 0.19(2) than previously measured values on single crystals (η = 0.07(1) [24,25]. Based on these results, one may presume that most of the atoms reside at the Ti substitutional site, in an essentially defects-free

environment. However, the reason for the increased value can be induced by the nature of the thin films (lattice mismatch between TiO_2 and Si) and generally formation of non-ideal crystal structure, on contrary to single crystals [24]. Furthermore, as the annealing and measurement were performed simultaneously in oxygen-lacking-atmosphere, it can facilitate formation of oxygen scarce regions, where certain deviations from stoichiometry could occur.

Table 1. ^{111m}Cd/Cd fitting parameters featuring the main EFGs fractions. ω_0 is given in Mrad·s^{-1}, δ (which is a relative width of a distribution) and perc. are in %, while V_{zz} numbers are presented in (10^{21} V·m^{-2}). EFG of the same origin are marked with colours. Spectra H_2-RT, H_2-423K and H_2-663K are fitted in one of the possible ways due to the complex local surroundings.

State:	**EFG:**	**Data:**				
		Perc.	ω_{0n}	η_{0n}	δ_{0n}	V_{zz}
Pristine	1	100	96.5(3)	0.19(2)	3.6(3)	6.38(2)
H_2-RT	2	8.4(5)	127.2(21)	0.37(8)	1.1(3)	8.41(2)
	3	27.7(46)	178.8(16)	0.46(2)	3.5(10)	11.82(3)
	4	63.9(71)	250.6(21)	0.39(1)	7.0(5)	16.56(4)
H_2-423K	5	38.2(75)	286.2(53)	0.68(2)	6.7(19)	18.91(4)
	1′	16.9(34)	94.7(18)	0.19(7)	4.2(8)	6.26(2)
	3′	44.9(41)	184.2(13)	0.83(2)	7.1(10)	12.17(2)
H_2-473K	5′	37.4(27)	295.3(10)	0.63(1)	1,3(1)	19.52(4)
	6	62.6(60)	292(14)	0.00	24.3(45)	19.31(9)
H_2-573K	5″	29.0(22)	296.2(6)	0.64(1)	0.6(1)	19.58(4)
	6′	71.1(24)	300.3(19)	0.57(2)	15.1(21)	19.85(4)
H_2-663K	5‴	9.6(32)	276.7(21)	0.81(1)	1.1(8)	18.29(4)
	7	66.2(71)	160.8(11)	0.54(2)	9.5(12)	10.63(3)
	8	24.2(46)	85.3(20)	0.75(3)	8,0(11)	5.64(2)

3.2. Hydrogenated at RT

After hydrogenation the spectra became remarkably complex and, without Fourier transform analysis, it would be challenging to distinguish amongst the variety of local environments/EFGs and their corresponding fractions. Upon hydrogenation treatment at RT, there is no evidence for EFG1. The spectrum was best fitted with the help of three EFG distributions, leading to a strongly damped R(t) function, which is evidence for Cd atoms in a variety of local environments, characterised by EFG2, 3 and 4. One may point, that the limit of solubility of deuterium in metal oxides is temperature dependent [27]; consequently, hydrogenation treatment at RT is likely not efficient to introduce and promote hydrogen deeply and homogeneously into the lattice. Thus, a possible scenario, leading to the current PAC results in such sample, hints the existence of complex of hydrogen-related defects. These defects, upon interaction with the Cd probe, lead to a plethora of local environments, whilst Cd could still reside at or near the Ti sites. The actual matching of the ^{111m}Cd atoms distribution regarding the distribution of hydrogen is unknown. Most likely, their relative distributions, of diffused hydrogen and implanted Cd are not homogeneously overlapping.

At the limit of the experimental resolving power—statistics-wise, the assigned EFG2 contributes with small 8.4(5)% of a relatively undamped perturbation function (i.e., the signature of a relatively regular defect configuration). EFG3 contributes with 28(5) and has close V_{zz} and η EFG parameters such as EFG2, but demonstrating a much wider distribution, i.e., revealing the increase of defects density nearby. EFG4, being the principal contribution to the perturbation function (64(7)%), lastly characterises a fairly broad EFG distribution with a different characteristic V_{zz} and η. EFG4 likely evidences severe disorder induced during hydrogenation, which could not recover fast enough to be observed during the first ∼1 h of measurements performed at 581 K, when most of the statistics contribute to the TDPAC measurement.

It would be difficult to say, without modelling of defects with theoretical calculations, what are the reasons of the observed EFGs. Regardless of that, although some preferential configurations of Cd related defects might prevail, these cannot be resolved due to the still high concentration of randomly distributed H atoms or H-related complex defects.

It is noteworthy that, the particular H-complex defect configurations formed during hydrogenation at RT, might be correlated with intrinsic defects in TiO_2 created during that process. We suggest that the "likely" high density of poorly diffusing hydrogen atoms in the TiO_2 lattice induces the generation of intrinsic defects. This situation leads to the formation of complex hydrogen-lattice defects that are stable enough to remain observable during the TDPAC measurements performed at 581 K. However, as soon as the sample is heated during hydrogenation most of such complex defects will not predominate, e.g., after hydrogenation at 423 K, as observed during the following TDPAC experiments. This fact suggests that temperature activated hydrogenation with enhanced H-diffusion reduces the number of H-complex defects as well as H-lattice correlated defects.

3.3. Hydrogenated at 423 K

Measurements performed on the sample hydrogenated at 423 K open a pathway for further discussions. The spectrum is analysed in terms of three broad EFG distributions, namely EFG1′, EFG3′ and EFG5. The corresponding R(t) function has a slightly clearer and more developed shape, though still shows evidence for the broad EFG distributions. Seemingly, the current hydrogenation temperature allowed to bring back a small 17(3)% fraction of EFG1 (designated here as EFG1′), which is characterised with similar to EFG1 V_{zz} and η electric field gradient parameters.

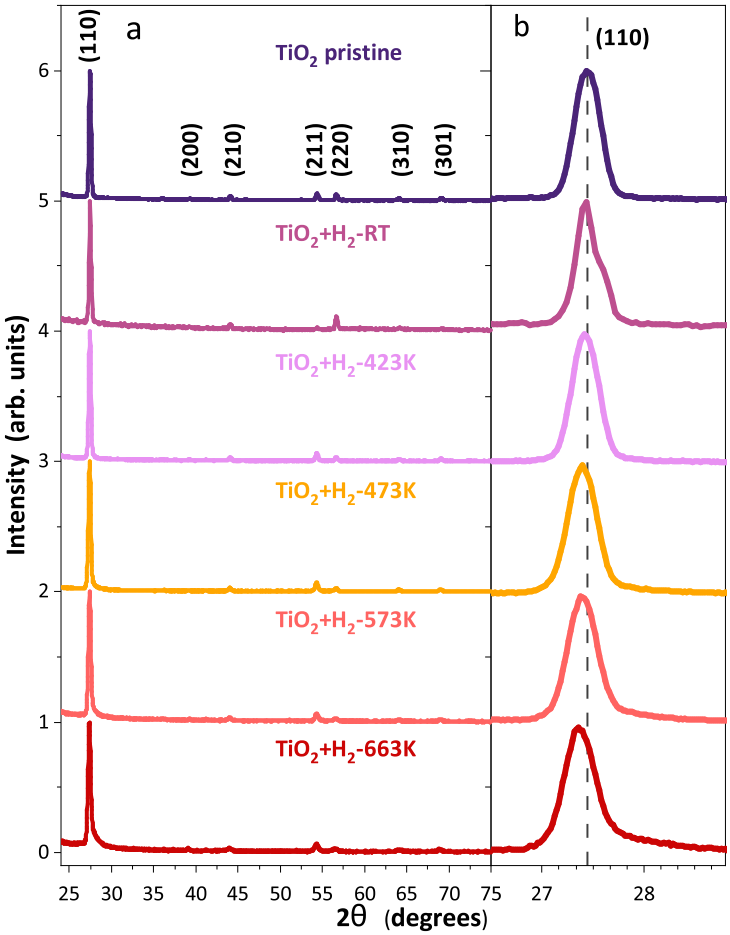

Figure 2. GIXRD patterns of hydrogenated rutile (**a**) and (**b**) the magnified (110) reflex demonstrating a gradual shift.

This fraction demonstrates a relatively narrow EFG distribution. The next component, EFG3′, may have the same nature as the one formed after hydrogenation at RT—EFG3. In comparison to EFG3, one may notice a growth of the principal contribution to the perturbation function from 28(5)% to 45(4)%, whilst V_{zz} and the wide distribution remain almost the same, δ_{03} = 3.5(1)% and $\delta_{03'}$ = 7(1)%.

Apparently, the complex defects change and lead to more axially asymmetric EFGs signatures, as seen through the growth of $\eta_{03'}$ up to 0.83. EFG5, characterised with V_{zz} = 18.91(4)^{21} V·m^{-2} and η_{05} = 0.68(2), may be due to the further temperature development during hydrogenation of the defect configuration responsible for EFG4, with a similar wide EFG distribution. However, significant changes in the main frequency and axial asymmetry parameters, between EFG4 and EFG5 require that by no ways Cd is interacting with the same defect complex. At this point, one may argue that hydrogenation performed at 423 K is not entirely efficient to avoid the formation of still, e.g., H-lattice highly stable defects. Therefore, the current temperature step and its evaluation is not entirely justified, as it can be treated in several possible ways due to the local complexity and absence of the defined frequencies. Regardless, at this stage the material seems to be less damaged that further allowed a certain recuperation of implantation defects at relatively H-free zones for the implanted ^{111m}Cd probe atoms. Possibly, bestowed energy during hydrogenation, leading to higher dilution and less complex defects, allows hydrogen to interact more freely with the Cd acceptors in multiple ways, as might be seen in the case of samples hydrogenated at higher temperatures.

3.4. Hydrogenated at 473 K

Upon hydrogenation at 473 K the corresponding R(t) function became even more well-defined and solely two different EFGs are needed for analysis (EFG5′ and EFG6). One can notice that EFG5′, with a surprisingly narrow distribution function contributing with 37(3)% to the R(t), has central V_{zz} and $\eta_{05'}$ EFG parameters which are quite close to the previously observed EFG5. Both EFG5′ and EFG6 bear similar V_{zz} parameters: 19.58(4) and 19.31(9)^{21} V·m^{-2}, respectively. While nevertheless, both the axial asymmetry parameter $\eta_{05'}$ = 0.63(1) differs from η_{06} = 0, as well as the relative attenuation parameter $\delta_{05'}$ = 1.3(1)% and δ_{06} = 24(2)%. EFG6 is obviously a representative of a set of ^{111m}Cd probes at a particular local defect configuration with axial symmetry η_{06} = 0, which is located in places with important density of randomly distributed defects. Even though it is not a trivial task to make analogies, the spectral shape resembles results previously observed in other hydrogenated semiconductors (GaP:H, InP:H and InSb:H) [28]. Moreover, it has been argued that Cd-H pairs in these semiconductors generally have η = 0, which could hint on the origin of EFG6 observed at this temperature.

3.5. Hydrogenated at 573 K

Following hydrogenation at 573 K, ^{111m}Cd implantation and subsequent measurement at 581 K, there is obvious evidence for the remnants of EFG5′, with a slightly decreased fraction, now designated as EFG5″. Undoubtedly, the defect interacting with the Cd at the origin of EFG6, characterised by V_{zz} = 19.31(9)^{21} V·m^{-2}, η_{06} = 0 and δ_{06} = 24(4)% is gone. A new predominant EFG6′, which still has a wide distribution and characterised with V_{zz} 19.85(4)^{21} V·m^{-2}, $\eta_{06'}$ = 0.57(2) and $\delta_{06'}$ = 15(2)% appears. Noteworthy is the fact that both Cd-defect configurations, EFG5″ and EFG6′, evolve now in places with lower concentration of randomly distributed defects (see Table 1). From IR studies performed by Lavrov et al., one could think that hydrogen could remain in the lattice up to 1173 K, if stabilised by an impurity or native defect in the local surrounding [6]. This might be only one factor explaining the lack of time dynamic effects observable in the R(t) spectra, due to H dynamics and trapping/de-trapping of H at the Cd probe atoms.

The presence of H-related defects and the further interactions with the Cd probe atoms do look highly stable at the measuring temperatures. These are probably complex defects, that act as deep traps for hydrogen and the Cd related probe atom, leading to no observable

dynamics on the atomic scale under the present experimental conditions. Nonetheless, one can be convinced that partial implantation damage annealing is happening within the first half an hour of the measurement, the actual relevance of the diluted concentration of Cd and associated defects on the present set of experiments, looks very much irrelevant, regarding the hydrogenation (damage and doping) effects for all processing temperatures.

3.6. Hydrogenated at 663 K

Hydrogenation at 663 K, with a following implantation of ^{111m}Cd probes and subsequent measurement at 573 K presents quite unexpected results. There are three different EFG distributions, with almost no traces of the previous Cd configurations, therefore we had to evaluate the data in the best feasible way due to a relatively damped spectrum and several possible ways to approach the data. Among the EFGs, there is the only one that resembles an already measured EFG, is EFG5″, although accounting for a reduced fraction of 10(3)%. However, EFG5″ could be of different nature, since diffusion of hydrogen is favourable at such hydrogenation temperatures as well as heavy reduction of the upper layers. This assertion could lead to formation of various non-stoichiometric phases (e.g., Magnéli phases or interstitial Ti). As the PAC measurements performed in vacuum, a chance of obtaining homogenous stoichiometric structure back is unlikely. Because of this, one may think that the temperature of hydrogenation was too high, seriously degrading the sample's upper layers with no possible recovery (e.g., turning them slightly amorphous). Regardless, results obtained by GIXRD measurements show no evidence of such effect (see Figure 2), and moreover demonstrate a shifting trend of the (110) reflection throughout treatments in the left-hand side.

The latter, was observed in ZnO doped with hydrogen and was attributed to hydrogen being incorporated into the lattice [29]. Based on the observed frequencies, one may assume that the family of observed EFG5 components are due to a combined complex, where one Cd atom is surrounded by the apical vacancy [24] and hydrogen. In order to perceive the exact location and chemical nature of the unique configuration, one needs to perform various DFT calculations. Preliminary calculations with the same supercell parameters as in Ref. [24], but including a substitution of V_o with H were proved to be inadequate, employing the standard PAW method in VASP environment. Therefore, performing large-scale quantum molecular dynamics simulations and explore other possible defects configurations are two ways to further investigate the systems under the scope [30].

4. Conclusions

First studies aiming to understand the building up of microscopic H-defect structures in TiO_2 thin films, upon various hydrogenation processes, were done with the help of PAC spectroscopy technique at ISOLDE/CERN. ^{111m}Cd probe atoms were implanted in the pre-processed TiO_2 thin films and subsequent measurements were carried out at 581 K. The PAC results demonstrate that different and specific Cd-H-defects configuration complexes exist or vanish essentially depending on the pre-processing hydrogenation temperature. The low hydrogenation temperature range (423–573 K) studied in the present work, seems to be not sufficient to recover the TiO_2 local structure, keeping a high density of complex H-defects, maybe also interacting with intrinsic defects created during hydrogenation. When compared with the results obtained on hydrogenated anatase, rutile demonstrates a different behaviour or, has the mechanism of dissociation which develops differently. While some defects show the corresponding EFG signatures, that could hint on the relevance of V_o and Cd-H paring, there is a necessity of a strong and comprehensive research simulation programme. Supported by quantum molecular dynamics, looking for the stabilisation of complex H-defect structures and then combining it with an extensive usage of VASP and WIEN2K first principle simulations we could expect to find matching hyperfine structure (EFG) parameters that can be compared and validated with the present set of PAC results.

Author Contributions: Conceptualization, J.S., P.S., and D.V.Z.; methodology, J.S. and J.G.M.C.; validation, J.G.M.C., J.S. and U.V.; formal analysis, D.V.Z. and J.G.M.C.; investigation, D.V.Z.; resources, J.S.; data curation, J.S. and U.V.; writing—original draft preparation, D.V.Z.; writing—review and editing, J.G.M.C. and P.S.; visualization, D.V.Z.; supervision, P.S.; project administration, P.S.; funding acquisition, P.S. and J.S. All authors have read and agreed to the published version of the manuscript.

Funding: This research was funded by the German Federal Ministry of Education and Research (BMBF) projects 05K19SI and 05K16PGA. Additional funding was obtained from the European Union's Horizon 2020 research and innovation program under grant agreement no. 654002 (ENSAR2). The authors are also grateful to CERN/ISOLDE for support of the experiment IS653. Support by the Center of Micro- and Nanotechnologies (ZMN), a DFG-funded core facility of TU Ilmenau and the Portuguese Science foundation FCT, via project CERN/FIS-TEC/0003/2019, are gratefully acknowledged.

Institutional Review Board Statement: Not applicable.

Informed Consent Statement: Not applicable.

Data Availability Statement: Data is available upon request.

Conflicts of Interest: The authors declare no conflict of interest.

Abbreviations

The following abbreviations are used in this manuscript:

PAC	Pertrubed Angular Correlation
EFG	Electric Field Gradient
GIXRD	Grazing incidence X-ray diffraction
CVD	Chemical Vapor Deposition
ICP	Inductively Coupled Plasma
TDPAC	Time-Differential Pertrubed Angular Correlation

References

1. Chen, X.; Liu, L.; Yu, P.Y.; Mao, S.S. Increasing Solar Absorption for Photocatalysis with Black Hydrogenated Titanium Dioxide Nanocrystals. *Science* **2011**, *331*, 746. [CrossRef] [PubMed]
2. Van de Walle, C.G.; Neugebauer, J. Universal Alignment of Hydrogen Levels in Semiconductors, Insulators and Solutions. *Nature* **2003**, *423*, 626–628. [CrossRef] [PubMed]
3. Setvin, M.; Franchini, C.; Hao, X.; Schmid, M.; Janotti, A.; Kaltak, M.; Van de Walle, C.G.; Kresse, G.; Diebold, U. Direct View at Excess Electrons in TiO_2 Rutile and Anatase. *Phys. Rev. Lett.* **2014**, *113*, 086402. [CrossRef] [PubMed]
4. Moses, P.G.; Janotti, A.; Franchini, C.; Kresse, G.; Van de Walle, C.G. Donor Defects and Small Polarons on the TiO_2(110) Surface. *J. Appl. Phys.* **2016**, *119*, 181503. [CrossRef]
5. Chester, P.F.; Bradhurst, D.H. Electrolytically Induced Conductivity in Rutile. *Nature* **1963**, *199*, 1056–1057. [CrossRef]
6. Herklotz, F.; Lavrov, E.V.; Weber, J. Infrared Absorption of the Hydrogen Donor in Rutile TiO_2. *Phys. Rev. B* **2011**, *83*, 235202. [CrossRef]
7. Koch, S.G.; Lavrov, E.V.; Weber, J. Photoconductive Detection of Tetrahedrally Coordinated Hydrogen in ZnO. *Phys. Rev. Lett.* **2012**, *108*, 165501. [CrossRef]
8. Chen, W.P.; Wang, Y.; Chan, H.L.W. Hydrogen: A Metastable Donor in TiO_2 Single Crystals. *Appl. Phys. Lett.* **2008**, *92*, 112907. [CrossRef]
9. Nandasiri, M.I.; Shutthanandan, V.; Manandhar, S.; Schwarz, A.M.; Oxenford, L.; Kennedy, J.V.; Thevuthasan, S.; Henderson, M.A. Instability of Hydrogenated TiO_2. *J. Phys. Chem. Lett.* **2015**, *6*, 4627–4632. [CrossRef]
10. Chen, Y.; Gonzalez, R.; Tsang, K.L. Diffusion of Deuterium and Hydrogen in Rutile TiO_2 Crystals at Low Temperatures. *Phys. Rev. Lett.* **1984**, *53*, 1077–1079. [CrossRef]
11. Spahr, E.J.; Wen, L.; Stavola, M.; Boatner, L.A.; Feldman, L.C.; Tolk, N.H.; Lüpke, G. Giant Enhancement of Hydrogen Transport in Rutile TiO_2 at Low Temperatures. *Phys. Rev. Lett.* **2010**, *104*, 205901. [CrossRef]
12. Schell, J.; Schaaf, P.; Lupascu, D.C. Perturbed Angular Correlations at ISOLDE: A 40 Years Young Technique. *AIP Adv.* **2017**, *7*, 105017. [CrossRef]
13. Johnston, K.; Schell, J.; Correia, J.G.; Deicher, M.; Gunnlaugsson, H.P.; Fenta, A.S.; David-Bosne, E.; Costa, A.R.G.; Lupascu, D.C. The Solid State Physics Programme at ISOLDE: Recent Developments and Perspectives. *J. Phys. G* **2017**, *44*, 104001. [CrossRef]
14. Forkel-Wirth, D.; Achtziger, N.; Burchard, A.; Correia, J.; Deicher, M.; Licht, T.; Magerle, R.; Marques, J.; Meier, J.; Pfeiffer, W.; et al. Hydrogen Passivation of Cd Acceptors in III-V Semiconductors Studied by PAC Spectroscopy. *Solid State Commun.* **1995**, *93*, 425–430. [CrossRef]

15. Dogra, R.; Byrne, A.P.; Ridgway, M.C. The Potential of the Perturbed Angular Correlation Technique in Characterizing Semiconductors. *J. Electron. Mater.* **2009**, *38*, 623–634. [CrossRef]
16. Zyabkin, D.V.; Gunnlaugsson, H.P.; Gonçalves, J.N.; Bharuth-Ram, K.; Qi, B.; Unzueta, I.; Naidoo, D.; Mantovan, R.; Masenda, H.; Ólafsson, S.; et al. Experimental and Theoretical Study of Electronic and Hyperfine Properties of Hydrogenated Anatase (TiO2): Defect Interplay and Thermal Stability. *J. Phys. Chem.* **2020**, *124*, 7511–7522. [CrossRef]
17. Das, S.K.; Thakare, S.V.; Butz, T. The Nuclear Quadrupole Interaction at ^{111}Cd and ^{181}Ta Sites in Anatase and Rutile TiO_2: A TDPAC Study. *J. Phys. Chem. Solids* **2009**, *70*, 778–781. [CrossRef]
18. Gunnlaugsson, H.P.; Mantovan, R.; Masenda, H.; Mølholt, T.E.; Johnston, K.; Bharuth-Ram, K.; Gislason, H.; Langouche, G.; Naidoo, D.; Ólafsson, S.; et al. Defect Annealing in Mn/Fe-implanted TiO_2(rutile). *J. Phys. D* **2014**, *47*, 065501. [CrossRef]
19. Jäger, M.; Iwig, K.; Butz, T. A compact digital time differential perturbed angular correlation-spectrometer using field programmable gate arrays and various timestamp algorithms. *Rev. Sci. Inst.* **2011**, *82*, 065105. [CrossRef]
20. Catherall, R.; Andreazza, W.; Breitenfeldt, M.; Dorsival, A.; Focker, G.J.; Gharsa, T.P.; Giles T, J.; Grenard, J.L.; Locci, F.; Martins, P.; et al. The ISOLDE Facility. *J. Phys. G* **2017**, *44*, 094002. [CrossRef]
21. Fromknecht, R.; Khubeis, I.; Massing, S.; Meyer, O. Ion Implantation in TiO_2: Damage Production and Recovery, Lattice Site Location and Electrical Conductivity. *Nucl. Instrum. Methods Phys. Res. Sect. B* **1999**, *147*, 191–201. [CrossRef]
22. Ziegler, J.F.; Ziegler, M.D.; Biersack, J.P. SRIM–The Stopping and Range of Ions in Matter. *Nucl. Instrum. Methods Phys. Res. Sect. B* **2010**, *268*, 1818–1823. [CrossRef]
23. Haas, H.; Röder, J.; Correia, J.G.; Schell, J.; Fenta, A.S.; Vianden, R.; Larsen, E.M.H.; Aggelund, P.A.; Fromsejer, R.; Hemmingsen, L.B.S.; et al. Free Molecule Studies by Perturbed $\gamma-\gamma$ Angular Correlation: A New Path to Accurate Nuclear Quadrupole Moments. *Phys. Rev. Lett.* **2021**, *126*, 103001. [CrossRef] [PubMed]
24. Zyabkin, D.V.; Schell, J.; Gaertner, D.; Dang, T.T.; Gonçalves, J.N.; Marschick, G.; Schaaf, P. Hyperfine Interactions and Diffusion of Cd in TiO_2 (Rutile). *J. Appl. Phys.* **2019**, *126*, 015102. [CrossRef]
25. Errico, L.A.; Fabricius, G.; Rentería, M. Metal Impurities in an Oxide: Ab Initio Study of Electronic and Structural Properties of Cd in Rutile TiO_2. *Phys. Rev. B* **2003**, *67*, 144104. [CrossRef]
26. Schell, J.; Zyabkin, D.; Lupascu, D.C.; Hofsäss, H.C.; Karabasov, M.O.; Welker, A.; Schaaf, P. A Hyperfine Look at Titanium Dioxide. *AIP Adv.* **2019**, *9*, 085208. [CrossRef]
27. Thomas, D.G.; Lander, J.J. Hydrogen as a Donor in Zinc Oxide. *J. Chem. Phys.* **1956**, *25*, 1136–1142. [CrossRef]
28. Baurichter, A.; Deicher, M.; Deubler, S.; Forkel, D.; Meier, J.; Wolf, H.; Witthuhn, W. Microscopical Studies at Cadmium Impurities in Compound Semiconductors. *Appl. Surf. Sci.* **1991**, *50*, 165–168. [CrossRef]
29. Gaspar, D.; Pereira, L.; Gehrke, K.; Galler, B.; Fortunato, E.; Martins, R. High Mobility Hydrogenated Zinc Oxide thin Films. *Sol. Energy Mater. Sol. Cells* **2017**, *163*, 255–262. [CrossRef]
30. Mattsson, T.R.; Root, S.; Mattsson, A.E.; Shulenburger, L.; Magyar, R.J.; Flicker, D.G. Validating Density-Functional Theory Simulations at High Energy-Density Conditions with Liquid Krypton Shock Experiments to 850 GPa on Sandia's Z Machine. *Phys. Rev. B* **2014**, *90*, 184105. [CrossRef]